IOSR Journal of Applied Geology and Geophysics (IOSR-JAGG)
e-ISSN: 2321–0990, p-ISSN: 2321–0982.Volume 10, Issue 1 Ser. I (Jan. – Feb. 2022), PP 57-68
www.iosrjournals.org

Analysis of Aster Imagery for Spectral Separability of Mineral Rock

Dahiru Mohammed Zakari[1],Ahmed Buba Seli[2]Simon Lee[3]
Nehemiah Japhet[4]
Department of Surveying & Geoinformatics[1,3,4]; Department of Civil Engineering[2]
Adamawa State Polytechnic Yola.
Corresponding Author: Dahiru Mohammed Zakari

Abstract:*The Advanced Spaceborne Thermal Emission and Reflection Radiometer (ASTER) data were utilised to construct lithological units and structural maps for a specific region in this experiment. Multispectral satellite images are used in earth science to analyse structure and hydrothermal change. Although gold cannot be identified directly by remote sensing methods, the presence of minerals with diagnostic spectrum signatures, such as iron oxides and clay minerals, can. The results of remote sensing techniques such as colour composite (CC), band ratio (BR), principal component analysis (PCA), and minimal noise fraction (MNF) have been assessed using a geological map of the area. In this work, the spatial filtering technique was applied by applying the directional spatial filter in three directions and generating a colour composite picture. This study made use of spectral mapping techniques such as MNF, SAM, MF, and MTMF. The suggested technique illustrates ASTER's strong potential in lithological unit identification employing nine bands of data (VNIR-SWIR). For modification zones, the least noise fraction approach was utilised, and the results were encouraging. The image was filtered using spectral angle mapper matched filtering and Mixture-Tuned Matched-Filtering, and the results were clear enough to indicate high prospective regions for gold mineralization in the future based on the spectral reflectance from the mines in the research area.*

Keywords– *Satellite Image, Spectral Signatures, hydrothermally altered rocks, Spectral Separability, Spectral Library.*

Date of Submission: 12-01-2022 Date of Acceptance: 27-01-2022

I. Introduction

Scientists investigate and measure physical reality (atmosphere, water, soil, and rock), live inhabitants (Homo sapiens, plants, and animals), and processes in action to discover these absolute notions (mass wasting, deforestation, and urban sprawl)(Kolie *et al.*, 2021).The scientists formulate a hypothesis and then attempt to accept or reject them in a systematic, unbiased fashion(Grüne-yanoff, 2021). The data necessary to accept or reject a hypothesis may be collected directly in the field, often referred to as *in situ* or place data collection (Tewes *et al.*, 2015)and from airborne and Spaceborne platforms that provide valuable information for research studies(Baldridge *et al.*, 2009). There is growing interest in how The Advanced Spaceborne Thermal Emission Reflection Radiometer (ASTER) on NASA's Terra Platform provide measurements that have been widely used in geological and other application (Pour and Hashim, 2011; Pour *et al.*, 2019) ASTER offers improved spatial, spectral and radiometric resolution. Hence, our purpose is to evaluate the utility of multispectral ASTER imagery in identifying and mapping different types of Geological Minerals. Five Rock minerals were specifically considered for spectral separability analysis and mapping: Calcite, Chlorite, Hematite, Kaolinite, and Muscovite(Herold *et al.*, 2004).

The ASTER sensor was developed in Japan by a combination of government, industrial, and research organisations. Every image is on a greyscale from black to white and is based on the brightness of radiation at a certain wavelength (between 0.52 and 11.65 µm) (Ourhzif *et al.*, 2019).Radiation reflected in the VNIR spectral band is included in ASTER data. Three recording channels with a spatial resolution of 15 m exist at wavelengths between 0.52 and 0.86 µm. To build a digital elevation model, band "B3" is separated into B3b and B3n utilising techniques developed by an ASTER scientific team (Janati *et al.*, 2014). These bands are employed for the differentiation of clays, phyllosilicates, and limestone and are effective for mapping chloritemetamorphic alteration. The shortwave length infrared (SWIR) contains six recording channels with wavelengths ranging from 1.6 to2.43 µm, with a spatial resolution of 30 m (Pour and Hashim, 2012). The TIR subsystem comprises five recording channels with wavelengths ranging from 8.125 to 11.65 µm and a spatial resolution of 90 m.

Because of their sensitivity to iron oxide minerals, VNIR wavelengths have been frequently employed for mineralization mapping (Mazhari *et al.*, 2017).

In the realm of ore minerals exploration, lithological and structural mapping, the Advanced Spaceborne Thermal Emission and Reflection Radiometer (ASTER), Advanced Land Imager (ALI), and Hyperion remote sensors are highlighted in this study. This study also discusses how digital image processing techniques might help geologists obtain the spectral data they need for their work.For the investigation of epithermal gold, porphyry copper, massive sulphide, chromite, magnetite, and uranium ore deposits, remote sensing equipment have been widely and effectively utilised to recognise hydrothermally altered minerals and lithological mapping (Pour and Hashim, 2011, 2014; Diefenderfer *et al.*, 2016; Basavarajappa *et al.*, 2019; Pour *et al.*, 2019; Xue *et al.*, 2021). Geological mapping and mineral prospecting were two of the most common applications during the early stages of remote sensing technology development (Tan and Qiao, 2020). This study intends to offer an overview of the usage of remote sensing data in the field of geological mapping, especially ASTER. To improve the capability of lithological discrimination between different rock units in the research region, digital processing, namely Band ratio, principal component analysis (PCA), and minimal noise fraction (MNF), will be used.

Mineral Rocks

A mineral is a naturally occurring material that is solid and stable at room temperature, has an organised atomic structure, is represented by a chemical formula, is generally abiogenic, and has a chemical formula. There are about 4,900 recognised mineral species, with the International Mineralogical Association (IMA) approving over 4,660 of them (Lesovik, 2014). Over 90% of the Earth's crust is made up of silicate minerals. The chemistry of the Earth governs the diversity and abundance of mineral species. Silicon and oxygen account for nearly 75% of the Earth's crust, resulting in the dominance of silicate minerals.

Minerals are differentiated by a variety of chemical and physical characteristics (Hazen *et al.*, 2013). Different species are distinguished by differences in chemical composition and crystal structure, and these qualities are impacted by the geological setting in which the mineral is formed. Minerals can be classified according to their physical qualities, which are related to their chemical structure and composition. Crystal structure and habit, hardness, lustre, diaphaneity, colour, streak, tenacity, cleavage, fracture, parting, and specific gravity are all common differentiating qualities (Karnataka-india, 2020). More specific mineral tests include acid reaction, magnetism, taste or smell, and radioactivity.

Spectral Library Building

The spectral library is utilised as a resource for identifying materials in remotely sensed photographs. The library's spectra can be matched using either the Advanced Space-borne Thermal Emission Reflection Radiometer (ASTER) spectral library or the United States Geological Survey (USGS) spectral library (Boori *et al.*, 2018).

Spectral library (USGS)

Using SWIR reflectance data, rocks were distinguished from non-hydrothermal silica-rich rocks (Ballance and Waiters, 2002). Calcite, dolomite, epidote, and chlorite generally display overlapping CO3 and Fe, Mg-O-H spectral absorption characteristics around 2.31-2.33 m, making it challenging to map them independently using SWIR data in prior research (Pour *et al.*, 2020). However, in the TIR, rocks containing calcite and dolomite show an 11.2 m spectral absorption signature, whereas epidote and chlorite-rich rocks show a 10.2 m spectral absorption signal (Mars and Rowan, 2011). Thus, ASTER TIR calcite-dolomite spectra have greater band 13 and lower band 14 emissivity, whereas epidote-chlorite TIR spectra have lower band 13 and higher band 14 emissivity. The calcite-dolomite and epidote-chlorite logical operators map the 2.31-2.33 m absorption feature using the ASTER SWIR band ratio 6/8 and the ASTER TIR band ratio 13/14 set to larger than 1 to map calcite-dolomite-rich rocks and less than 1 to map epidote-chlorite-rich rocks (Basavarajappa *et al.*, 2019). Each logical operator algorithm generates a byte picture, which is then translated to a shapefile for use in Arc-GIS.

Spectral Library (ASTER)

As part of the ASTER efforts, a (Version 1.2) library containing over 2000 spectra of natural and man-made materials was developed and compiled as the ASTER spectral library in 1998, and over 4000 copies of the spectral have been sent to over 90 nations since that time (Baldridge *et al.*, 2009).The JPL section of the ASTER spectral library has been considerably revised, and the library's version number has been raised to Version 2. This collection has around 2300 spectra. Additional spectra from 0.4-15.4um of 100 rocks samples are included, as are new measurements of the original 160JPL mineral samples present in version1.2 of the collection. There is no new material from the USGS or Johns Hopkins University collections. ASTER measures reflected

radiation in three bands in the 0.52-0.86 m wavelength region (VNIR), six bands in the 1.6-2.43 m wavelength region (SWIR), and five bands of emitted radiation in the 8.125-11.65 m wavelength region (TIR), with resolutions of 15 m, 30 m, and 90 m, respectively. ACORN atmospheric correction software was used to adjust ASTER VNIR and SWIR radiance data to reflectance data (Mars and Rowan, 2011).

Using ENVI's atmospheric removal and emissivity normalisation techniques, TIR radiance measurements were calibrated to emissivity data. Using Interactive Data Language (IDL) logical operators, rocks containing hydrothermal silica, calcite-dolomite, epidote-chlorite, alunite-kaolinite, and sericite were mapped. IDL logical operators connect band thresholds and band ratios to map mineral spectral characteristics (Meerdink *et al.*, 2019). In IDL logical operators, ASTER SWIR band ratios are employed to map the Al-O-H spectral absorption properties of alunite, kaolinite, and sericite. The ASTER SWIR 4/5 ratio corresponds to the 2.165 m spectral absorption feature in alunite and kaolinite, whereas the ASTER SWIR 4/6 and 7/6 ratios correspond to the 2.2 m spectral absorption feature in alunite, kaolinite, and sericite (Pour and Hashim, 2014). ASTER SWIR and ASTER TIR band ratios were used to map hydrothermal silica. The ASTER SWIR band ratio of 4/7 is often greater for hydrothermal silica-rich rocks, which exhibit lower overall SWIR reflectance in the 2.0 to 2.4 m area due to residual molecular water or an O-H absorption feature spanning 2.26 to 2.4 m, than for non-hydrothermal silica-rich rocks. The quartz restrain absorption feature at 9.09 m is mapped using the ASTER TIR band ratio 13/12 (Guha and Vinod Kumar, 2016). Thus, silica-rich rocks and hydrothermal silica-rich rocks were mapped using TIR emissivity data.

II. Sample Measurement

The ASTER library continues to be one of the most extensive collections of spectra encompassing the wavelength range 0.4-15um (Baldridge *et al.*, 2009) (Fig.1a) and indicating spectra of minerals, rocks, lunar and terrestrial soils, materials, manufactured plants, snow, and ice. The solar spectral range 0.4-2.5um (Fig.1a) contains a wealth of information regarding a wide range of key earth-surface minerals. The 2.0-2.5 µm SWIR spectral region, in particular, encompasses spectral characteristics of hydroxyl-bearing minerals, sulphates, and carbonates that are common to numerous geological units and hydrothermal alteration assemblages (Pour *et al.*, 2019).

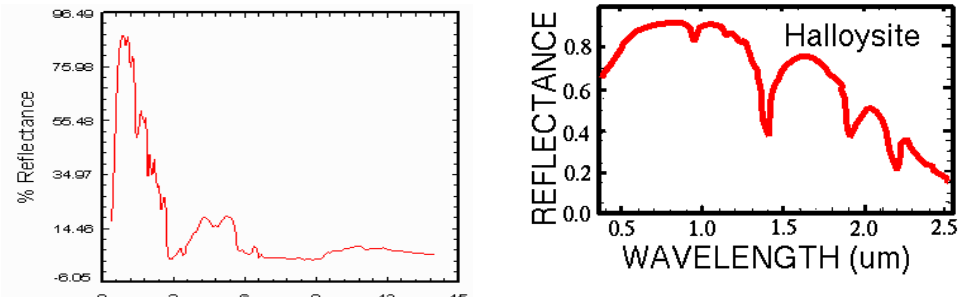

a **b**

Figure 1. The ASTER spectral libraryconsists of data from three other spectral libraries.

The spectral library's version 1.2 provides hemispheric reflectance data of minerals recorded with the Beckman UV5240 spectrophotometer from 0.4 to 2.5 m. Minerals with different spectral properties, such as kaolinite, alunite, muscovite, and pyrophyllite, play essential roles in natural resource discovery and characterisation. ASTER is a multi-spectral imager that can see in the following wavelength ranges: visible and near-infrared (VNIR, 0.4-1.0 m), short-wavelength infrared (SWIR, 1.0-2.4 m), and thermal infrared (TIR, 8-12 m) (Baldridge *et al.*, 2009).

- The Johns Hopkins University (JHU) Spectral Library
- The Jet Propulsion Laboratory (JPL) Spectral Library, and
- The United States Geological Survey (USGS – Reston) Spectral Library.

The Jet Propulsion Laboratory (JPL) Spectral Library

The mineral samples used to construct the JPL mineral spectra ranging from 0.4 to 15.5 m were procured from a variety of sources, including Ward's Natural Science Establishment, Burnham Mineral Company, and others. The JPL rock spectra were generated using rock samples from the ward's 100 North American Rock collection, which has 100 specimens of the most volcanic, metamorphic, and sedimentary rocks. (Pour and Hashim, 2011).

III. Material and Methods

Remote sensing data

A cloud-free Aster Imagery was used in this study. The images were processed and analyzed by ENVI (Environment for Visualizing Images) 5.3, Erdas Imagine 2014 and GIS 10.2 software packages(Theses and Reports, 2018).

Data Processing

The software was used to analyze the laboratory data and manage the spectral library through the following links to the official data series, which include; Description of how spectral were measured, Sample purity, Full sample description, and Plot of the spectral and through the ASCII window in the software.

Measurement Technique in The Electromagnetic Spectrum

Standard X-ray Diffraction analysis was used to evaluate the purity and composition of each mineral sample (Chen, 2018). The Diffraction line was recognised by comparing it to the mineral powdered Diffraction file search manual and data book. These spectra, which range from 2.08 to 25 µm, cannot be utilised to forecast emissivity quantitatively since only hemispherical reflectance can be employed in this manner. Except for sections of generic snow and vegetation spectra, all other spectral data were recorded in directional hemispherical reflectance with a sample interval of 0.001µm from 0.4 - 0.8 µm and 0.004 µm from 0.8-2.5 µm. Most of the time, the infrared part of this data may be utilised to determine emissivity using Kirchhoff's Law (E=1-R), which has been validated by laboratory and field experiments. However, when correctly recorded, as stated in the meteorite study, the curve form is precise enough for remote sensing applications (Kuenzer *et al.*, 2014).

ASTER Instrument Characteristics

ASTER is a multispectral sensor with 14 bands that can measure reflectance and emitted electromagnetic radiation from the earth's surface in three subsystems consisting of:

- Visible and near-infrared radiation (VNIR), with a spatial resolution of Three bands 0.52-0.86um
- Shortwave infrared radiation (SWIR) Six band 1.6-2.43um
- Thermal infrared radiation (TIR),8.125-11.65um wavelength region are 15 and 30 and 90m, [12][1]. As shown in the next table 1

Table 1. ASTER instrument characteristics (Yamaguchi et al., 1999).

Characteristic	VNIR	SWIR	TIR
Spectral range (µm)	Band 1: 0.52–0.60, Nadir looking Band 2: 0.63–0.69, Nadir looking Band 3: 0.76–0.86, Nadir looking Band 3: 0.76–0.86, Backward looking	Band 4: 1.600– 1.70 Band 5: 2.145– 2.185 Band 6: 2.185– 2.225 Band 7: 2.235– 2.285 Band 8: 2.295– 2.365 Band 9: 0.360– 2.430	Band 10: 8.125–8.475 Band 11: 8.475–8.825 Band 12: 8.925–9.275 Band 13: 10.25–10.95 Band 14: 10.95–11.65
Ground resolution (m)	15	30	90
Swath width (km)	60	60	60
Singnal quantization level (bits)	8	8	12

Minerals Rock and Their Properties

The United States Geological Survey is actively mapping minerals linked with hydrothermal alteration in a research region that encompasses the majority of the United States Basin and Range. A mineral can be recognised by numerous physical features, some of which are sufficient for unambiguous identification. Crystal structure and habit, hardness, lustre, diaphaneity, colour, streak, cleavage and fracture, and specific gravity are all physical qualities used for categorization (Minerals, 2004). Fluorescence, phosphorescence, magnetism, radioactivity, and tenacity are other less broad tests (response to mechanical induced changes of shape or form), The most evident attribute of a mineral is its colour, yet it is frequently non-diagnostic. It is caused by the interaction of electromagnetic radiation with electrons. In terms of their contribution to the colour of a mineral, two major types of elements are identified. Idiochromatic elements are fundamental to the composition of minerals; their contribution to the colour of minerals is diagnostic. Malachite (green) and azurite are two examples of such minerals (blue)(Assessment, no date). (http://en.wikipedia.org/wiki/Mineral).

Calcite (Aragonite)

Many creatures on Earth would be extinct if calcite and aragonite did not exist. These are the minerals that most invertebrates employ to build their shells and hard parts (Addadi and Weiner, 2014). So, if you've ever appreciated a colourful seashell, you've already paid homage to the variety of colours calcite and aragonite come in, as well as, indirectly, the ease with which calcite and aragonite originate at the Earth's surface. Aragonite and calcite are 'polymorphs,' or minerals that have similar chemical compositions but somewhat different crystal shapes(Diamond and River, no date). Both minerals may coexist and are so similar that distinguishing them is rarely essential for anybody other than a professional geologist. Calcite may be found in several settings, such as hot springs and underground tunnels, as well as forming coral reefs and seashells(Reeder, 1996). This shows not just the quantity of calcite, but also the ease with which it forms, dissolves, and reforms. Calcite is virtually as prevalent in modern culture as it is in nature, with applications ranging from medicine and animal feed to Michelangelo's "Pieta" to highway overpasses(Arbor and Haven, 2012).

Description and Identifying Characteristics

Calcite comes in both crystalline and massive forms. Calcite crystals are usually transparent to translucent, but if microscopic impurities are present, they can show a wide spectrum of colours. Calcite masses are generally light in colour, although as with transparent crystals, even little amounts of impurities can yield a wide range of colours (Gettenst and Fitzhugh, 1974) Fig. (a-d).

Chemical / physical Properties

Ca (CO3), Mn Fe, Mg are transparent to translucent calcite crystals that are colorless, white, or light-colored(Pour and Hashim, 2014; Jr, 2016).

The chlorite

SWIR-identified chlorite compositions also exhibit consistent variations with the amount of alteration and distance from ore (Xue *et al.*, 2021). In rhyolitic samples near ore, the average wavelength of the FeOH absorption feature for chlorite is 2,241 nm (middle Mg chlorite), whereas wavelengths in background samples average 2,247 nm (intermediate Fe chlorite). The average wavelength of the FeOH absorption characteristic for chlorite in rhyolitic samples near ore is 2,241 nm (middle Mg chlorite), whereas wavelengths in background samples average 2,247 nm (intermediate Fe chlorite) (Jones *et al.*, 2005).

Chemical / Physical properties

The chlorite group's common members are represented by this formula ((Mg, FeLi)6 AlSi3 O10(OH)8) (Assessment, no date). They are bright to dark green, greyish-green, and black. White, yellow-brown, pink, and purple are some of the colour variations; it is also transparent to translucent. They are most commonly found in metamorphic environments, as well as as a secondary mineral in volcanic basalt. Sediment Chlorite Alteration Chlorite alteration is frequently observed in sediments (a possible sign of mineralization proximity?) 'Chloritic' sediments have a greenish tint to them. Lower AlOH wavelength (2198nm versus 2205 – 2209nm) compared to 'unaltered' sediments (Ballance and Waiters, 2002) Figure (a-d);

• 'Ironstone' rock types are quartz-rich or quartz-poor (not always visually apparent)
• 'Chlorite alteration' of sediments is considered an important indicator of proximity to alteration associated with mineralization. 'Greenish' sediments are not necessarily chlorite-altered
• Some changes in AlOH (white mica) composition noted in different sediments;
• Unaltered sediments 2205 – 2209nm
• 'chlorite altered sediments are around 2198nm.

Hematite

Hematite is undoubtedly one of the most important elements of Martian interest for a variety of reasons. Hematite is a ferrous oxide (-Fe2O3) that occurs naturally in two colours: red and grey, depending on the granulometry of the samples (Wang *et al.*, 2008). The red variety is common on Earth: it is rust, which produces easily when the iron is exposed to air.Pure crystalline hematite particle samples with grain sizes ranging from 0.1m to 10m (hereafter normal red hematite samples) have reflectance spectra that are saturated (near zero) in the violet and ultraviolet and climb sharply throughout the visible (Marra *et al.*, 2005). This behaviour explains the characteristic red colour of this kind of hematite, which is a mineral form of the resource iron. The ore ranges in colour from black to steel to reddish-brown. There are several kinds, including kidney ore, martite, and iron rose.

Chemical/Physical properties

Iron (III) Oxide, Fe_2O_3 a-Fe_2O_3, they are red-reddish brown, steel-grey to black, and reddish-brown to blackFigure 3(a-d).

Kaolinite Al_2 (Oh)$_4$ (Sio_5)

Kaolinite is a clay mineral, part of the group of industrial minerals, with the chemical composition $Al_2Si_2O_5(OH)_4$(Eomo and Logy, 1889)(Quang Minh and Hoc Thang, 2020). It is a layered silicate mineral, with one tetrahedral sheet linked through oxygenatoms to one octahedral sheet of alumina octahedral Kaolinite is a clay mineral that is formed by the weathering of feldspar. It is one of the most common minerals found in all parts of the Earth. It is very soft with a hardness of 2-2.5. and has a colour of white, pink or grey and a streak of white. The chemical make-up is Al2 Si2 O5 $(OH)_4$(Schulze, 2018). Kaolinite is used in the ceramics industry for the production of clay productsFigure 4(a-d).

Muscovite

Muscovite is the most common mica, either as a contact metamorphic rock or as a secondary mineral emerging from the alteration of topaz, feldspar, kyanite, and other minerals. It is frequently discovered in enormous sheets that are economically useful in pegmatite Figure 2. (a-d).

Chemical/Physical properties

Vitreous, Silky, Pearly, Transparent, and Translucent are some of the adjectives used to describe this material. They are also colourless and silvery-white in appearance. (OH)2 Kal2 (AlSi3O10) (Diamond and River, no date).

IV. Experimental Result Analysis and Discussion

The ASTER SWIR subsystem's six spectral bands were designed to measure reflected solar radiation to distinguish AL-OH, Fe Mg-OH, Si-O-H, and CO3 absorption features (Pour *et al.*, 2020), in previous research carried out for the identification of some of the hydrothermal alteration minerals through analysis of ASTER SWIR data, which have been demonstrated using in situ field spectrum measurements; as a result, these qualities make SWIR of ASTER data appropriate for thorough mineralogical alteration mapping, which is critical for distinguishing the high potential regions of economical mineralization of ore deposits. These multispectral zones contain minerals with diagnostic spectral absorption properties in the SWIR section of the electromagnetic spectrum that may be distinguished from one another using ASTER SWIR data (van der Meer *et al.*, 2014; Khorram *et al.*, 2016).

The broad phyletic zone (fine grain metamorphic rock with well-developed luminous) is characterised by illite/muscovite (sericite) that exhibits an intense Al-OH absorption feature centred at 2.20 m, which corresponds to ASTER band 6, and the narrow argillic (sedimentary rock formed from consolidated clay) zone, which includes kaolinite and muscovite that exhibits absorption features at 2.2um, which corresponds. The mineral assemblage of the outer propylitic zone consists of epidote (a glossy yellow-green mineral composed of calcium, aluminium, and iron silicate), chlorite, and calcite, which display absorption characteristics at 2.35 m that correlate with ASTER band 8 Fig 10 (Pour *et al.*, 2019). This will suggest a more promising place with a profitable mineralization zone (Herold *et al.*, 2004). In this research exercise, spectral mapping methods such as SAM were used on SWIR ASTER data to identify particular hydrothermal alteration zones associated with porphyry copper deposits in the region.

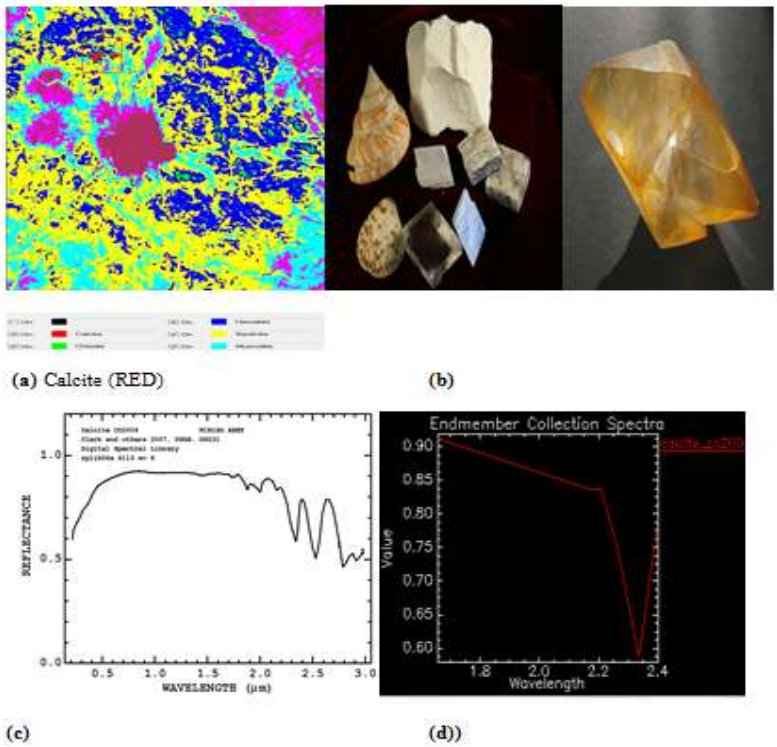

igure 2(a,b): Exhibit absorption feature situated in the 2.35um that coincide with ASTER band 8

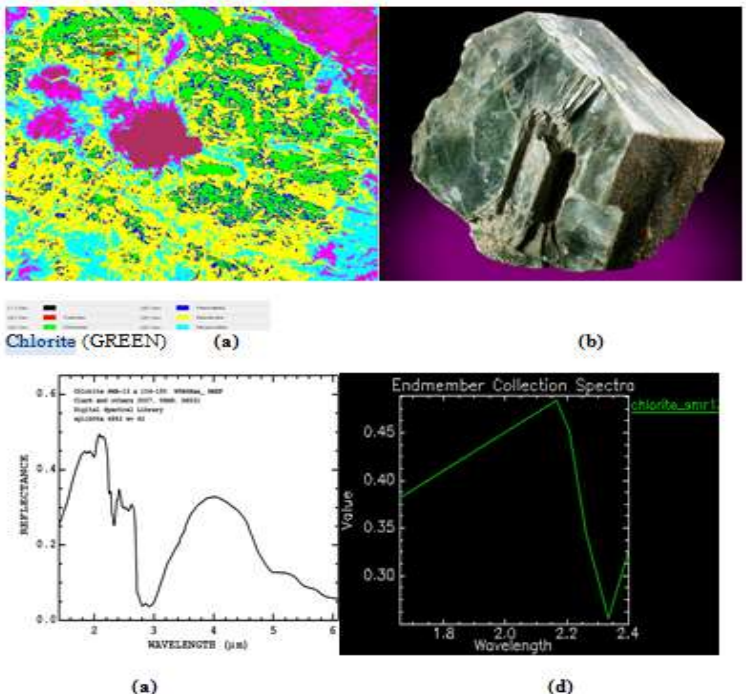

Figure 3.(a-d) (a) Exhibit absorption feature situated in the2.35 µm that coincide with ASTER band 8.

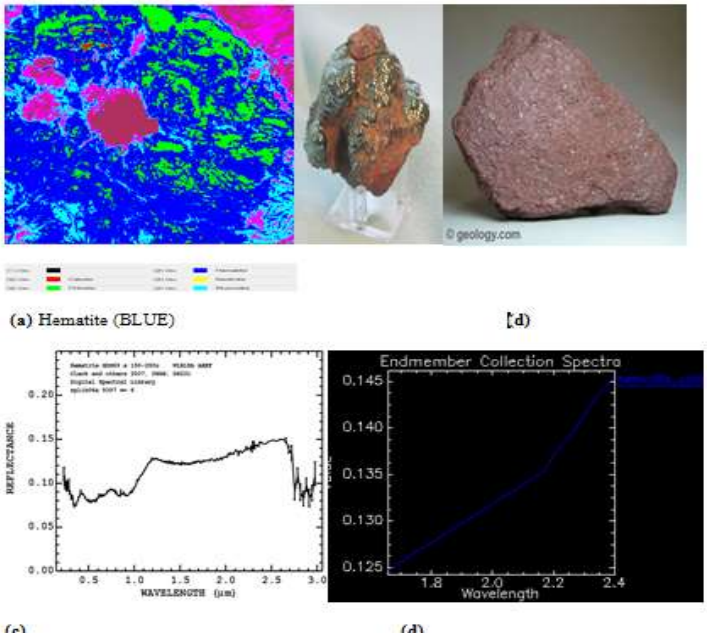

Figure 4(a-d) ***Exhibit*** reflectance spectra which are saturated (near zero) in the violet and ultraviolet and steeply increase throughout the visible:

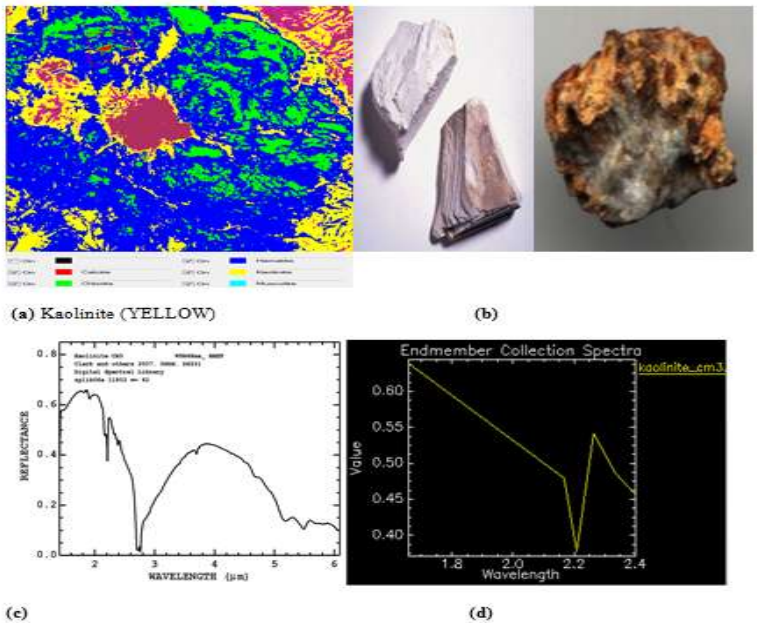

Figure 5(a-d) Kaolinite displayed absorption at 2.20 µm correspond with band 5

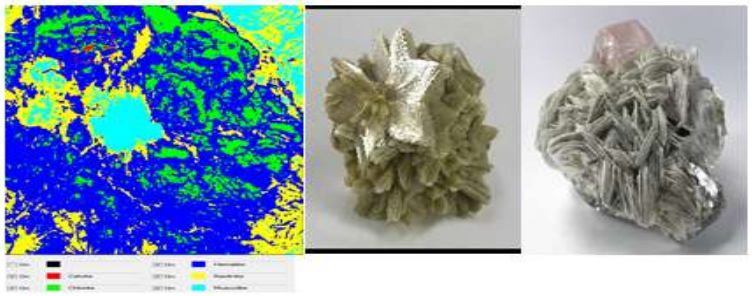

(a) Muscovite (CYAN) (b)

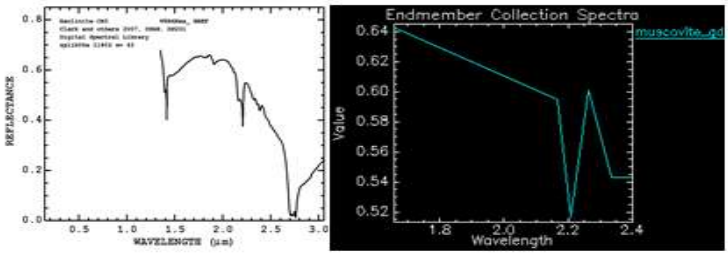

(c) (d)

'igure 6 (a-d) Muscovite displayed absorption at 2.20 µm correspond with band 5

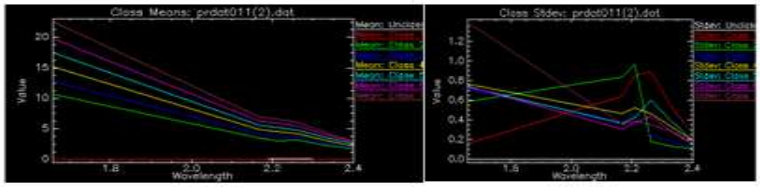

Figure :(6a) Class Mean **(b) Class Stdev**

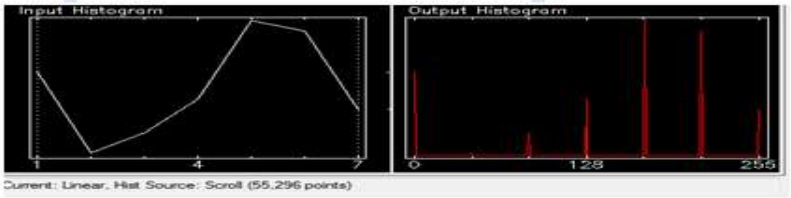

Figure: (7a-b) Histograms Stretching **(b)**

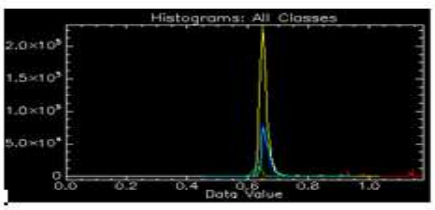

Figure: (8) Histograms: All Classes

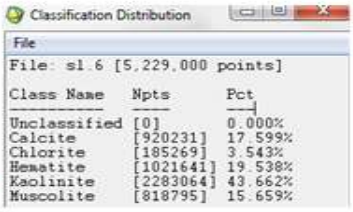

Table 2. Class Distribution

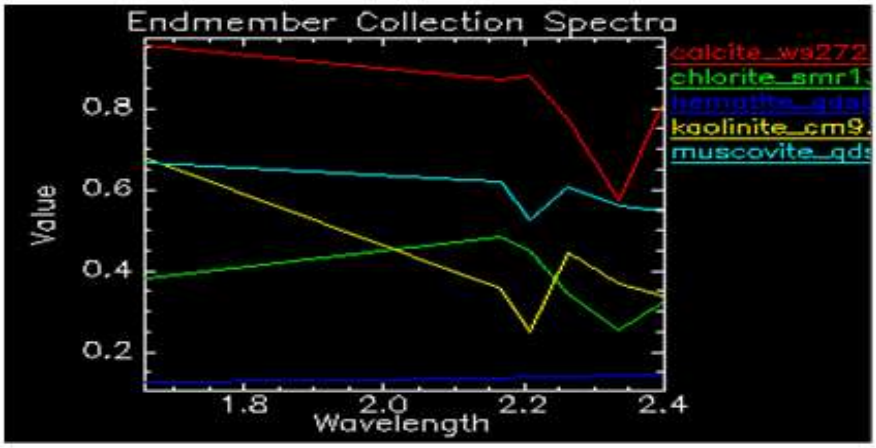

Figure: 9 Laboratory spectra of calcite, chlorite, Kaolinite, and muscovite resampled to ASTER bandpasses. Spectra include Calcite and chlorite exhibit absorption features situated in the 2.35um that coincide with ASTER band 8: kaolinite and Muscovite display absorption feature at 2.20 µm correspond with ASTER band 5.

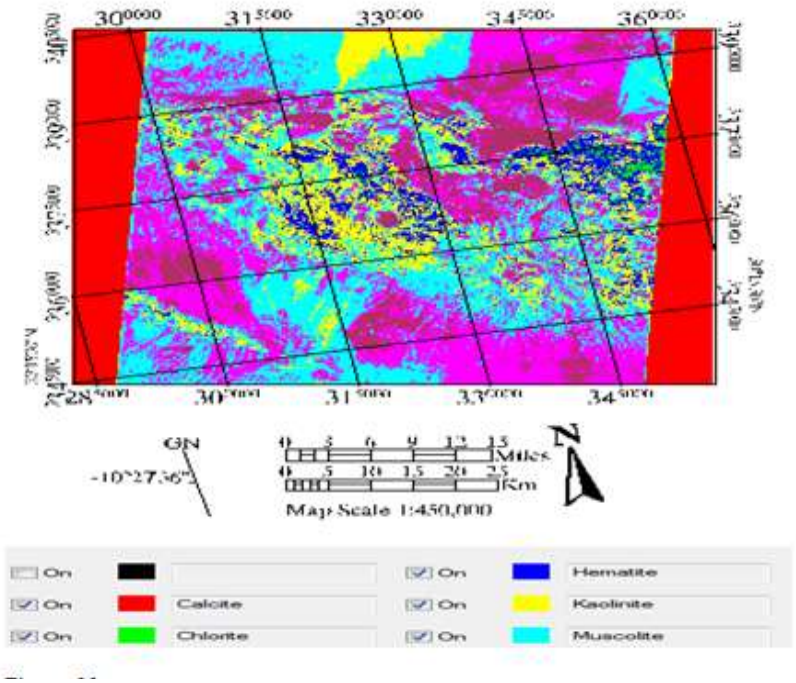

Figure 10. Spectral Separability Map

V. Results and Discussion

The spectral angle mapper (SAM) was chosen as the tool for mapping the surface composition in this study. SAM is a physically-based classification technique that analyses the spectral similarity of surface reflection images and reference spectra, considering them as vectors in a space with dimensions equal to the number of bands (Kiran Raj *et al.*, 2015). An image map illustrating the distribution and abundance of chosen minerals was created using a spectral Angle mapper (SAM). SAM categorization image maps for the two chosen locations are shown in Figures (a,b,c).

VI. Conclusion

This study investigated the applicability of ASTER data for lithologic mapping and discovered that the important lithologic group's Calcite, chlorite, Hematite, Kaolinite, and Muscovite can be identified effectively from ASTER data. However, we suggest further study should look at other sensors like Landsat 8 OLI/TIR and Sentinel 2 for the lithological mapping

References

[1]. Addadi, L. and Weiner, S. (2014) 'Biomineralization: Mineral formation by organisms', *Physica Scripta*, 89(9).
[2]. Arbor, A. and Haven, N. (2012) 'N n n n', 26(2009), pp. 1–3.
[3]. Assessment, A. F. P. (no date) *Century Porcelain Analysis*.
[4]. Baldridge, A. M., Hook, S. J., Grove, C. I. and Rivera, G. (2009) 'The ASTER spectral library version 2.0', *Remote Sensing of Environment*. Elsevier Inc., 113(4), pp. 711–715.
[5]. Ballance, P. F. and Waiters, W. A. (2002) 'Hydrothermal alteration, contact metamorphism, and authigenesis in Ferrar Supergroup and Beacon Supergroup rocks, Carapace Nunatak, Allan Hills, and Coombs Hills, Victoria Land, Antarctica', *New Zealand Journal of Geology and Geophysics*, 45(1), pp. 71–84.
[6]. Basavarajappa, H. T., Jeevan, L., Rajendran, S. and Manjunatha, M. C. (2019) 'Aster Mapping of Limestone Deposits and Associated Lithounits of Parts of Chikkanayakanahalli, Southern Part of Chitradurga Schist Belt, Dharwar Craton, India', *Journal of the Indian Society of Remote Sensing*. Springer India, 47(4), pp. 693–703.
[7]. Boori, M. S., Paringer, R. A., Choudhary, K. and Kupriyanov, A. V. (2018) 'Comparison of hyperspectral and multi-spectral imagery to building a spectral library and land cover classification performance', *Computer Optics*, 42(6), pp. 1035–1045.
[8]. Chen, L. (2018) 'Thermal decomposition characterization of supergene potassium- jarosite and sodium-jarosite minerals from the northern Tibetan', 54(2), pp. 459–466.
[9]. Diamond, M. B. and River, M. (no date) 'Macle of'.
[10]. Diefenderfer, J., assumptions Vipin Arora, M. and Singer, L. E. (2016) *International Energy Outlook 2016 Liquid fuels*, *Doe/Eia-0484*.
[11]. Eomo, R. O. G. and Logy, P. H. O. (1889) 'CHAPTER 4 H Y D ROG EOMO R PHO LOGY 4 .al.
[12]. Gettenst, R. J. and Fitzhugh, E. W. (1974) 'Calcium Carbonate Whites Author (s): Rutherford J . Gettens, Elisabeth West Fitzhugh and Robert L . Feller Published by : Taylor & Francis, Ltd . on behalf of the International Institute for Conservation of Historic and Artistic Works Stable URL : https://www.jstor.org/stable/1505661 REFERENCES Linked references are available on JSTOR for this article : reference # references _ tab _ contents You may need to log in to JSTOR to access the linked references .', 19(3), pp. 157–184.
[13]. Grüne-yanoff, T. (2021) 'Justifying method choice : a heuristic-instrumentalist account of scientific methodology', *Synthese*. Springer Netherlands, 199(1), pp. 3903–3921.
[14]. Guha, A. and Vinod Kumar, K. (2016) 'New ASTER derived thermal indices to delineate mineralogy of different granitoids of an Archaean Craton and analysis of their potentials concerning Ninomiya's indices for delineating quartz and mafic minerals of granitoids-An analysis in Dharwar Cr', *Ore Geology Reviews*. Elsevier B.V., 74, pp. 76–87.
[15]. Hazen, R. M., Sverjensky, D. A., Azzolini, D., Bish, D. L., Elmore, S. C., Hinnov, L. and Milliken, R. E. (2013) 'Clay mineral evolution', *American Mineralogist*, 98(11–12), pp. 2007–2029.
[16]. Herold, M., Roberts, D. A., Gardner, M. E. and Dennison, P. E. (2004) 'Spectrometry for urban area remote sensing - Development and analysis of a spectral library from 350 to 2400 nm', *Remote Sensing of Environment*, 91(3–4), pp. 304–319.
[17]. Janati, M. El, Soulaimani, A. and Hefferan, K. P. (2014) 'Application of ASTER remote sensing data to geological mapping of basement domains in arid regions : a case study from the Central Anti-Atlas , Iguerda inlier , Morocco', pp. 2407–2422.
[18]. Jones, S., Herrmann, W. and Gemmell, J. B. (2005) 'Short wavelength infrared spectral characteristics of the HW horizon: Implications for exploration in the Myra Falls volcanic-hosted massive sulfide camp, Vancouver Island, British Columbia, Canada', *Economic Geology*, 100(2), pp. 273–294.
[19]. Jr, A. E. S. (2016) 'Minerals from the Miarolitic Cavities at the', 7529(September).
[20]. Karnataka-india, K. (2020) 'Review on characterization of minerals 1', V(2), pp. 1468–1475.
[21]. Khorram, S., van der Wiele, C. F., Koch, F. H., Nelson, S. A. C. and Potts, M. D. (2016) *Principles of applied remote sensing*, *Principles of Applied Remote Sensing*.
[22]. Kiran Raj, S., Ahmed, S. A., Srivatsav, S. K. and Gupta, P. K. (2015) 'Iron oxides mapping from E0-1 hyperion data', *Journal of the Geological Society of India*, 86(6), pp. 717–725.
[23]. Kolie, B., Jun, Y., Sunahara, G. and Camara, M. (2021) 'Characterization of the rock blasting process impacts in Lefa gold mine , Republic of Guinea', *Environmental Earth Sciences*. Springer Berlin Heidelberg, 80(5), pp. 1–17.
[24]. Kuenzer, C., Ottinger, M., Wegmann, M., Guo, H., Wang, C., Zhang, J., Dech, S. and Wikelski, M. (2014) 'Earth observation satellite sensors for biodiversity monitoring: potentials and bottlenecks', *International Journal of Remote Sensing*. Taylor & Francis, 35(18), pp. 6599–6647.
[25]. Lesovik, V. S. (2014) 'Architectural Geonics Subject and Tasks', *Journal of Engineering and Architecture*, 2(2), pp. 263–266.
[26]. Marra, A. C., Blanco, A., Fonti, S., Jurewicz, A. and Orofino, V. (2005) 'Fine hematite particles of Martian interest: absorption spectra and optical constants', *Journal of Physics: Conference Series*, 6, pp. 132–138.
[27]. Mars, J. C. and Rowan, L. C. (2011) 'ASTER spectral analysis and lithologic mapping of the Khanneshin carbonatite volcano , Afghanistan', (1), pp. 276–289.
[28]. Mazhari, N., Shafaroudi, A. M. and Ghaderi, M. (2017) 'Detecting and mapping different types of iron mineral- ization in Sangan mining region, NE Iran, using satellite image and airborne geophysical data', 21(1), pp. 137–148.
[29]. van der Meer, F., Hecker, C., van Ruitenbeek, F., van der Werff, H., de Wijkerslooth, C. and Wechsler, C. (2014) 'Geologic remote sensing for geothermal exploration: A review', *International Journal of Applied Earth Observation and Geoinformation*. Elsevier B.V., 33(1), pp. 255–269.
[30]. Meerdink, S. K., Hook, S. J., Roberts, D. A. and Abbott, E. A. (2019) 'Remote Sensing of Environment The ECOSTRESS spectral library version 1 . 0', *Remote Sensing of Environment*. Elsevier, 230(May), p. 111196.
[31]. Minerals, N. E. W. (2004) 'Agardite- (Ce)', 42, pp. 1901–1927.
[32]. Ourhzif, Z., Algouti, Ahmed, Algouti, Abdellah and Hadach, F. (2019) 'LITHOLOGICAL MAPPING USING LANDSAT 8 OLI AND ASTER MULTISPECTRAL DATA IN IMINI-OUNILLA DISTRICT SOUTH HIGH ATLAS', XLII(June), pp. 10–14.
[33]. Pour, A. B. and Hashim, M. (2011) 'The Earth Observing-1 (EO-1) satellite data for geological mapping, southeastern segment of the Central Iranian Volcanic Belt, Iran', *International Journal of Physical Sciences*, 6(33), pp. 7638–7650.
[34]. Pour, A. B. and Hashim, M. (2012) 'The application of ASTER remote sensing data to porphyry copper and epithermal gold deposits', *Ore Geology Reviews*. Elsevier B.V., 44, pp. 1–9.
[35]. Pour, A. B. and Hashim, M. (2014) 'ASTER , ALI and Hyperion sensors data for lithological mapping and ore minerals exploration'.
[36]. Pour, A. B., Hashim, M., Hong, J. K. and Park, Y. (2019) 'Lithological and alteration mineral mapping in poorly exposed lithologies using Landsat-8 and ASTER satellite data: North-eastern Graham Land, Antarctic Peninsula', *Ore Geology Reviews*. Elsevier B.V., 108, pp. 112–133.

[37]. Pour, A. B., Park, Y., Hong, J. K., Muslim, A. M. and Pradhan, B. (2020) 'Listvenite occurrences in the fault zones of northern Victoria Land, Antarctica: Aster-based mapping approach', *40th Asian Conference on Remote Sensing, ACRS 2019: Progress of Remote Sensing Technology for Smart Future*, (Acrs), pp. 1–7.
[38]. Quang Minh, D. and Hoc Thang, N. (2020) 'Characteristics of Novel Geopolymer Composites Synthesized from Red Mud and Diatomaceous Earth in Autoclave Conditions without Using Alkaline Activators', *Journal of Polymer & Composites*, (December).
[39]. Reeder, R. J. (1996) 'Interaction of divalent cobalt, zinc, cadmium, and barium with the calcite surface during layer growth', *Geochimica et Cosmochimica Acta*, 60(9), pp. 1543–1552.
[40]. Schulze, D. G. (2018) 'An introduction to soil mineralogy', *Soil Mineralogy with Environmental Applications*, 7(7), pp. 1–35.
[41]. Tan, K. and Qiao, J. (2020) 'Development history and the prospect of remote sensing technology in coal geology of China', *International Journal of Coal Science & Technology*. Springer Singapore, 7(2), pp. 311–319.
[42]. Tewes, A., Thonfeld, F., Schmidt, M., Oomen, R. J., Zhu, X., Dubovyk, O., Menz, G. and Schellberg, J. (2015) 'Using RapidEye and MODIS data fusion to monitor vegetation dynamics in semi-arid rangelands in South Africa', *Remote Sensing*, 7(6), pp. 6510–6534.
[43]. Theses, M. and Reports, M. (2018) 'Digital Commons @ Michigan Tech OIL SPILLS DETECTION utilizing UAS AND INEXPENSIVE AIRBORNE THERMAL SENSORS'.
[44]. Wang, W., Howe, J. Y. and Gu, B. (2008) 'Structure and morphology evolution of hematite (α-Fe 2O3) nanoparticles in forced hydrolysis of ferric chloride', *Journal of Physical Chemistry C*, 112(25), pp. 9203–9208.
[45]. Xue, Q., Wang, R., Liu, S., Shi, W., Tong, X., Li, Y. and Sun, F. (2021) 'Significance of chlorite hyperspectral and geochemical characteristics in exploration: A case study of the giant Qulong porphyry Cu-Mo deposit in collisional orogen, Southern Tibet', *Ore Geology Reviews*. Elsevier B.V., 134(April), p. 104156.

Dahiru Mohammed Zakari, et. al. "Analysis of Aster Imagery for Spectral Separability of Mineral Rock."*IOSR Journal of Applied Geology and Geophysics (IOSR-JAGG),* 10(1), (2022): pp 57-68.